TECHNICAL TRANSACTIONS | CZASOPISMO TECHNICZNE
MECHANICS | MECHANIKA
4-M/2015

ANDRZEJ TROJNACKI*, BOGDAN SZYBIŃSKI*

INVESTIGATIONS OF STRENGTH AND LEAK TIGHTNESS OF WAVE-RING GASKETS

BADANIA WYTRZYMAŁOŚCI I SZCZELNOŚCI USZCZELEK DWUFALISTYCH

Abstract

The paper deals with stress-strain analysis and estimation of leak tightness of *wave-ring* gaskets. The investigations are carried out using the simplified analytical approach. A cylindrical shell of constant mean thickness is introduced to simulate the gasket. It is assumed that the shell is simply supported at the inner surface of the seat. The influence of certain geometric and assembly parameters on the strength and leak tightness of the closure is analytically investigated. The results are presented in dimensionless variables in order to generalise the conclusions. The analytical solution is verified by FEM calculations and compared with the experimental results.

Keywords: high-pressure closures, wave-ring gasket, stress-strain analysis

Streszczenie

W artykule przedstawiono analizę wytrzymałościową oraz ocenę szczelności uszczelek *dwufalistych* (typu „B"). W rozważaniach wykorzystano uproszczone podejście analityczne. Uszczelka została zamodelowana powłoką cylindryczną o stałej grubości, podpartą obwodowo na wewnętrznej powierzchni gniazda. Badano wpływ niektórych geometrycznych i montażowych parametrów złącza na wytrzymałość uszczelki oraz szczelność połączenia. W celu uogólnienia wyników zostały one przedstawione w funkcji zmiennych bezwymiarowych. Wyniki rozwiązania analitycznego zostały zweryfikowane za pomocą MES i porównane z wynikami badań doświadczalnych.

Słowa kluczowe: uszczelki wysokociśnieniowe, uszczelka typu "B", analiza wytrzymałościowa

DOI: 10.4467/2353737XCT.15.345.4866

* PhD. Andrzej Trojnacki, PhD. DSc. Bogdan Szybiński, Institute of Machine Design, Faculty of Mechanical Engineering, Cracow University of Technology.

1. Introduction

Modern power installations and advanced chemical equipment, usually operating at extremely high pressures, require reliable and hard-wearing sealing systems. Metal gaskets are sometimes used to seal the heads of reactors or boilers and pipe connections [1]. Metal gaskets give satisfactory sealing service, and additionally, they are chemically resistant, moisture-proof and heat stable. Temporary closures with self-sealing metal *wave-ring* gaskets are applied in heavy-duty systems, in particular in these of great diameter.

The paper follows earlier contributions of the authors devoted to the sealing systems with metal gaskets for the high-pressure applications. Several computational models of the wave-ring gasket were investigated [5] with the aim of selecting the simplest and most effective one, but also sufficiently precise to be applied in the engineering approach. The results of the analysis confirm that the shell model of constant thickness simply supported at both ends at the inner surface of the seat is appropriate to describe the wave-ring gasket and leads to good agreement with FEM modelling. However, the seat must be considered as a thick-walled cylinder loaded by shear forces and internal operating pressure. The created analytical model was used to determine the influence of several gasket parameters on its strength and sealing properties [12]. The results of analysis were compared with FEM (ANSYS®) calculations and were verified by experimental results obtained under assembly conditions in the gasket installation state [7–10].

2. Engineering example and service conditions of the sealing

The wave-ring gasket is a certain type of self-sealing gaskets for very high-pressure equipment. An engineering example of the joint with wave-ring gasket between the vessel wall and reactor head is shown in Fig. 1. The closure is successfully applied [18] in the heavy-duty chemical installation working at the pressure of 200 MPa.

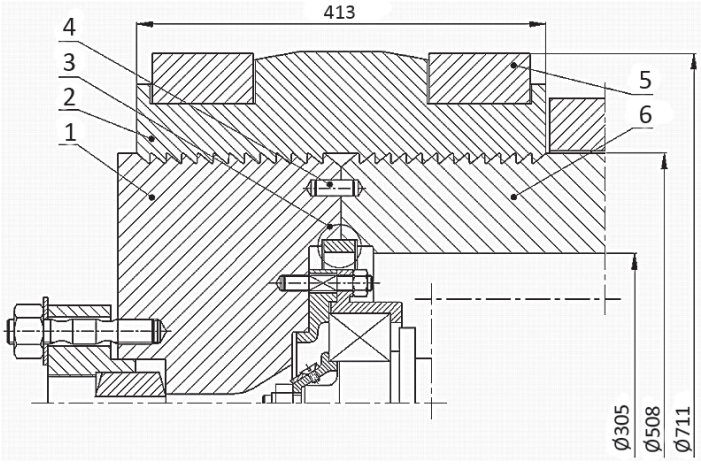

Fig. 1. Engineering example of the joint between the vessel wall and reactor head: 1 – head, 2 – sectional clamping rings, 3 – wave-ring gasket, 4 – locating pin, 5 – grips, 6 – cylindrical shell

The yield stress of the wave-ring gasket material must be significantly lower than the yield stress of the seat material to ensure the proper effectiveness of the joint. The gasket is usually made of low-carbon soft steel subjected to heat refining to the yield limit of approximately 400 MPa. Sometimes, the gasket is manufactured out of copper, brass, or some other moderately soft metal. The high-quality chromium-nickel-molybdenum steel hardened to the yield limit of minimum 750 MPa is mostly used for the seats. The gasket must be made slightly oversized, so that an interference fit is obtained in the seat. The experience gained from testing of existing and properly running closures leads to the conclusion that the degree of the preferred radial interference between the external wave surface of the gasket and the cylindrical internal surface of the seat may vary from 0.5‰ to 2.5‰, and it depends on both the yield limit of the gasket material and the operating pressure.

Under assembly conditions, the initial contact pressure q appears at the portion e of a wave surface due to the assembly interference, thus making the initial seal just before the operating pressure p is applied to the closure (Fig. 2). The working pressure is exerted on the entire inner surface, forcing a seal on the two outer radii. The initial assembly pressure q increases as the stiffness of the gasket is much less than that of the seat. Because of its specific features, such a sealing can be applied in equipment working at extremely high pressure, far exceeding 100 MPa.

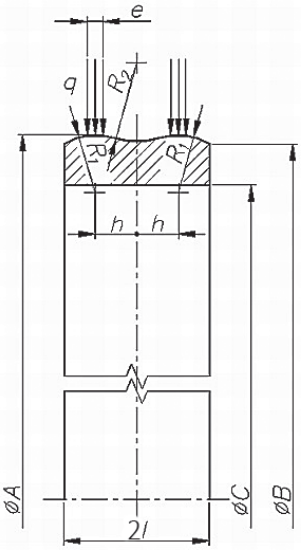

Fig. 2. Distribution of initial load at the contact region of the gasket

The difference in the yield limits of materials of the gasketed members and the value of the radial interference fit are the key parameters of the closure. They have an essential influence on the width of the contact zone of required size and on the related contact pressure value, which provides the leak tightness of the connection under the operating pressure p. In simple preliminary calculations of practical engineering applications of wave-ring gaskets, the non-leakage condition is usually formulated as:

$$q_{m\,opr} > R_{0.2g} \geq 2p \tag{1}$$

where the average contact pressure $q_{m\,opr} = 2q_{\max\,opr}/3$ as for the parabolic elastic distribution due to the Hertz theory. Because of highly approximate estimation of the contact stress distribution, the average value of the distribution is introduced into equation (1). It means that the average contact pressure $q_{m\,opr}$ in the contact zone under operating conditions must be greater than the yield limit $R_{0.2\,g}$ of the gasket material and should exceed the operating pressure p at least twice. The magnitude of the yield limit of the gasket material and the size of the radial interference fit are related and strongly depend on the applied operating pressure. The influence of several parameters of the connection on its sealing properties in the operating conditions was investigated in dimensionless variables [12]. The dimensionless non-leakage parameter was defined as $\psi = q_{m\,opr}/2p$ and the simplified analytical approach was applied to obtain the solution.

Wave-ring gaskets give satisfactory service where the vessel, or piping, does not need to be opened very often. Otherwise, they are somewhat impractical as they sometimes become so tightly wedged that the vessel head can be removed only with extreme difficulty. When this jamming occurs, the gasket usually must be discarded, as the crests have been flattened and scarred. Where the closure must be opened and closed fairly often, the gasket is sometimes made of hardened steel.

In conclusion, it should be noted that there are no design objectives and constraints collected, which can be recommended in the design procedures of the closures with wave-ring gaskets. The parameters of the new connections are selected basing on the experience gained during operation and improvements of the existing sealing systems. Moreover, in each individual case of technical application, a set of expensive and time-consuming calculations and experimental tests should be carried out to confirm the accuracy of the choice. A sudden unexpected decrease of the leak tightness of very high-pressure installation operating with caustic dangerous packing may cause serious damages.

3. Simplified analytical solution

The geometry of the investigated closure is presented in Fig. 3. For the analytical calculations, the gasket is replaced with a cylindrical shell of constant thickness t and mean radius r, where t is defined as an arithmetic average of three extreme values of gasket thickness. The analytical investigations of a gasket are then based on a simple shell model of length $2l$ simply supported around the circumference at contact with the seat. The hinges are selected at the top points of the wave surface where the contact with the seat occurs.

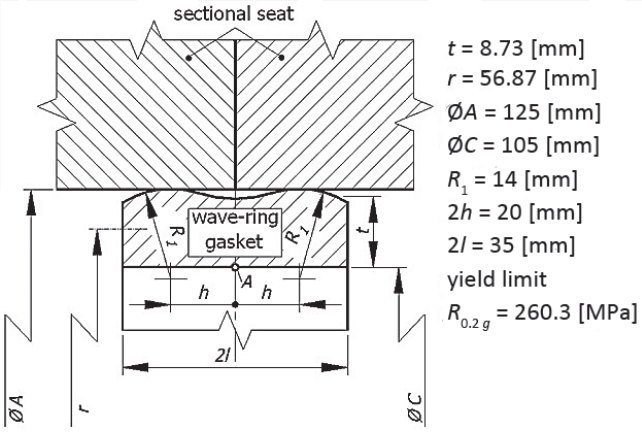

Fig. 3. Geometry of the closure with wave-ring gasket in assembly conditions (operating pressure $p = 0$)

The spacing of the supports is $2h$ (Fig. 4). It is assumed that, except a small region in the vicinity of supports, the shell is purely elastic. The analytical calculations verified by FEM

modelling lead to the conclusion that the influence of external parts of the gasket outside of the supports (broken line in Fig. 4) is negligible. The relative difference in maximum equivalent stress σ_{eq} at the inner surface of the gasket is less than 2% for this simplified model, with respect to the complete shell model with attached external segments. The results of the analysis confirm that the shell model of constant thickness simply supported at both ends at the inner surface of the seat in the cross-sections of coordinates $x = -h$ and $x = h$ is appropriate for the description of the wave-ring gasket and leads to a good agreement with FEM modelling. At the assembly conditions, the shell is loaded by shear forces Q_x at the supports only. Under service conditions, the shell is additionally loaded by an operating pressure p acting at the inner cylindrical surface and at the edge plain surfaces. The seat must be considered as a thick-walled cylinder loaded by shear forces and by the internal pressure p.

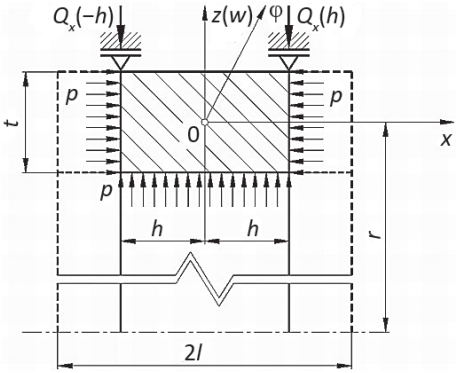

Fig. 4. Simplified computational model of the wave-ring gasket in service conditions

The applied approach, together with the permissible simplifications, depends in the shell theory on the geometric proportions of an element [14, 16]. In this case, the gasket must be solved on the basis of the bending shell theory and some terms in the differential equation of deflection could not be neglected. Under the assumptions as for the cylindrical axisymmetric shell of mean thickness t, mean radius r and small radial deflections w with respect to the thickness t, the differential equation of deflection takes the well-known form [2, 11]:

$$\frac{d^4w}{dx^4} + \alpha\frac{d^2w}{dx^2} + \beta^4 w = \delta \tag{2}$$

where:

$\alpha = \nu/r^2$,

$\beta = \sqrt[4]{12(1-\nu^2)/r^2t^2}$,

$\delta = 12p(1-\nu^2)/Et^3$,

ν and E – Poisson's ratio and Young's modulus, respectively.

The constants of integration can be determined from the boundary conditions as for the simply supported shell, and eventually, the shell model of the gasket can be easily solved. The principal stresses σ_z, σ_φ and σ_x can be expressed in terms of the shell parameters and operating pressure p. The maximum equivalent von Mises stress σ_{eq} occurs at the inner surface at the gasket's midpoint and is:

$$\sigma_{eq} = \sqrt{\sigma_z^2 + \sigma_\varphi^2 + \sigma_x^2 - \sigma_z\sigma_\varphi - \sigma_\varphi\sigma_x - \sigma_x\sigma_z} \tag{3}$$

The sectional seats (Fig. 3) are usually executed directly in thick vessel walls like in the example of closure shown in Fig. 1. These walls are designed for very high pressure and their thickness ratio is of great value. Nevertheless, the resultant displacement w_h (negative) at the support after assembly is different from the designed radial interference δ. The resultant displacement w_h was finally determined basing on the thick-walled cylinders theory applied to the shell model of the gasket and to the seat, respectively [13]:

$$|w_h| = \frac{\delta}{2}\frac{\kappa_2^2 - 1}{\kappa^2 - 1}\left[\kappa_1^2(1-\nu) + 1 + \nu\right] \tag{4}$$

where $\kappa_1 = (2r + t)/(2r - t)$ is the ratio between the outer and inner radii of the shell, κ_2 is the ratio between the outer and inner radii of the seat and κ stands for the thickness ratio of the entire unit. The pressure q at the contact surface of the cylinders corresponding to the interference δ is:

$$q = \frac{E\delta}{2r + t}\frac{\left(\kappa_1^2 - 1\right)\left(\kappa_2^2 - 1\right)}{\kappa^2 - 1} \tag{5}$$

and can be additionally used to estimate the shear force at the support:

$$Q_x = \frac{1}{2}2ql \tag{6}$$

Special attention must be paid to the interaction conditions between the wave working surface of the gasket and the cylindrical surface of the seat (Fig. 2). Initial assembly interference Δ is usually of a high value (more than 0.5‰), and the difference in mechanical properties of the materials may cause the plastic process in the gasket. For this reason, the Hertz theory cannot be used directly to calculate the width of the contact region, where the sealing is obtained.

Hypothetical elastic distribution of the contact stress $q(x)$ under operating pressure p is shown in Fig. 5a. In the regions where stress q calculated from the initial elastic Hertz distribution is considerably beyond the yield limit $R_{0.2\,g}$ of the gasket material, the plastic process must appear. As a result, redistribution of the initial elastic stress $q(x)$ must occur and finally resultant stress distribution $q_{pl}(x)$ must appear, which allows for plastic deformations (Fig. 5b).

Simple and rough estimation of width e of the contact region is derived on the assumption that the gasket material satisfies pure elastic-plastic stress-strain relationship and that the seat material is perfectly rigid. Moreover, it is assumed that plastic deformation begins when the gasket is subjected to load $Q_x(h)$, which produces stress $q_{max} = R_{0.2\,g}$. Under the load that produces stress q_{max}, which is n – times greater than the yield limit $R_{0.2\,g}$ ($q_{max} = nR_{0.2\,g}$), the elastic parabolic distribution $q_{el}(x)$ corresponding to the load $Q_{x\,el}(h) \le Q_x(h)$ will exist in the contact surface, for which the maximum stress equals $q_{max\,el}$. The width of the contact region satisfying this elastic Hertz distribution $q_{el}(x)$, with respect to the distribution $q(x)$ is:

$$e_{el} = \frac{1}{n}e \tag{7}$$

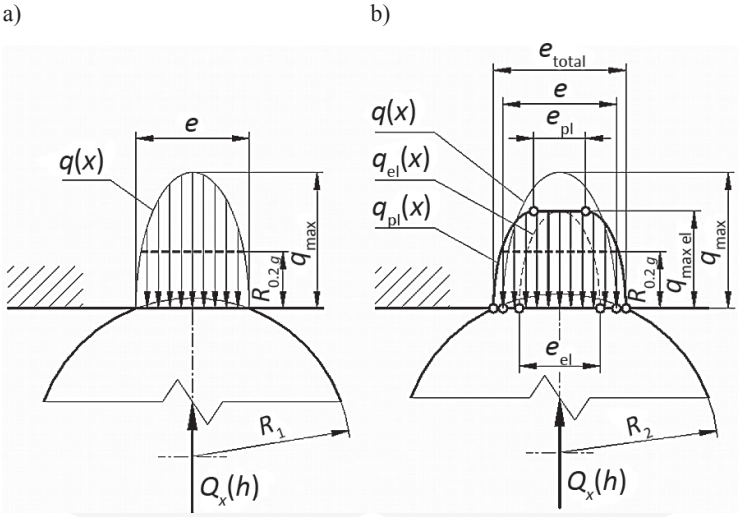

Fig. 5. Distribution of stress at the contact region of gasket and seat: a) hypothetical elastic (parabolic) with respect to the Hertz theory, b) changed (partially-linear) with respect to plastic deformation

The surplus shear load $\Delta Q_x(h) = Q_x(h) - Q_{x\,\mathrm{el}}(h)$ produces a plastic process, which leads, on the applied assumptions, to plastic deformation. A new partially-linear stress distribution $q_{\mathrm{pl}}(x)$ is introduced to model the problem (Fig. 5b). The width of the additional plastic zone is determined from the condition that the entire shear force $Q_x(h)$ does not change:

$$e_{\mathrm{pl}} = \frac{2}{3}\left(n - \frac{1}{n}\right)e \tag{8}$$

The total width of the contact region is then a sum of the elastic contact e_{el} (7) and plastic contact e_{pl} (8):

$$e_{\mathrm{total}} = \left(2n + \frac{1}{n}\right)\frac{e}{3} \tag{9}$$

The suggested simplified distribution of the contact stress $q_{\mathrm{pl}}(x)$ must be treated as a highly approximate one. The assumption of the pure elastic-plastic stress-strain curve of the gasket material leads to the overestimation of the total width of the contact region.

4. Numerical modelling (FEM)

Three parts of the investigated structure are assembled with an interference fit between the external wave surface of the gasket and the inner cylindrical surface of both seats. The

shape of the structure and relatively high radial interference, which should preserve the leak tightness of the junction under operating pressure, result in high stresses and stress gradients distributed over the small zones in the vicinity of contacting areas. The problem considered in the paper concerns the contact of two deformable bodies and belongs to the class of *flexible-to-flexible* contact, for which the analytical solutions are known only in a limited number of simple cases. Nowadays, the contact tasks are solved numerically, by means of the finite element approximation. The ANSYS® code [17] was used to solve the problem in the present paper and to get the strain and stress distributions in all contacting bodies. Also, the contact pressure distribution and the width of the contact zone were the results of this analysis.

The gaskets were made of soft 25CrMo4 (1.7218) chromium-molybdenum normalised steel and the seats were made of 42CrMo4 (1.7225) high-carbon chromium-molybdenum steel toughened to R_m = 1000 MPa. The mechanical properties of 25CrMo4 and 42CrMo4 steels were verified experimentally. Two cylindrical specimens were subjected to the same heat treatment as the corresponding elements, and prepared for the static tensile tests. The obtained real load-displacement curves $F = f(\Delta l)$ for both materials are shown in Fig. 6. The strength properties of both materials, calculated as arithmetic means of the two tests, are given in Table 1. The experimentally verified Brinell hardness number of the sealing surfaces of the gaskets was of 250–280 BHN and Rocwell hardness number of the seats was of 45–48.

Table 1

Uniaxial tension test results

Steel	E [MPa]	$R_{0.05}$ [MPa]	$R_{0.2}$ [MPa]	R_m [MPa]	$\varepsilon_{0.05}$ [%]	$\varepsilon_{0.2}$ [%]	ε_{max} [%]
25CrMo4 (N)	2.014×10^5	253.59	260.30	523.38	0.185	0.359	15.338
42CrMo4 (T)	2.064×10^5	809.12	812.46	918.50	0.460	0.711	8.802

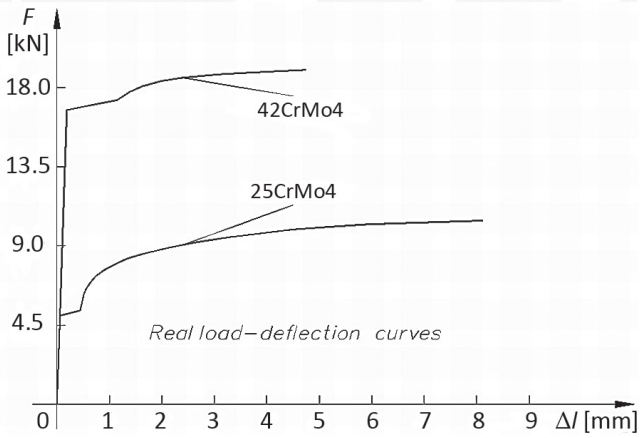

Fig. 6. Results of static tensile tests of 25CrMo4 (N) and 42CrMo4 (T) materials – real load-displacement curves $F = f(\Delta l)$ (not to scale)

Two approximations of the real stress-strain curves $\sigma = f(\varepsilon)$ of the materials used for the gasket and the seats were adopted in the paper. The parameters of the first multi-linear approximation (Fig. 7a) were calculated from the set of equations (10):

$$\begin{aligned} R_m - R_{0.2} - E_{t2}\left(\varepsilon_{\max} - \varepsilon_{0.2}\right) &= 0 \\ R_{0.2} - R_{0.05} - E_{t1}\left(\varepsilon_{0.2} - \varepsilon_{0.05}\right) &= 0 \\ R_{0.05} - E\varepsilon'_s - E_{t1}(\varepsilon_{0.05} - \varepsilon'_s) &= 0 \\ S_c - E\varepsilon'_s &= 0 \end{aligned} \tag{10}$$

and are given in Table 2. The parabolic modelling was suggested beyond the yield limit in the second approximation (Fig. 7b). The parabola containing the point of coordinates $\varepsilon_{0.2}$, $R_{0.2}$ and reaching the maximum value at the point $\varepsilon_{\max}$, R_m was applied to describe the tensile behaviour of the material. For the numerical calculations, the parabola was replaced by several (twenty) segments of different slope, but of equal length in the orthogonal projection at the ε axis. Such approximation enables direct introduction of the nonlinear material properties in the software module ANSYS®, which was used in the paper. Both approximations are conservative beyond the yield limit, although the second one is more precise. The similar approximation was proposed for the material used for the seats. However, plastic deformations were present in the softer part of the junction, namely in the gasket only.

Table 2

Parameters of the stress-strain curves approximation of the materials

	Steel	S_c [MPa]	ε'_s [%]	ε_s [%]	E_{t1} [MPa]	E_{t2} [MPa]
Gasket	25CrMo4 (N)	251.35	0.1248	0.159	3854.02	1756.37
Seat	42CrMo4 (T)	808.26	0.3916	0.511	1329.88	1310.63

Moreover, it was assumed that the relationship between equivalent stress σ_{eq} and equivalent strain ε_{eq} under complex stress states $\sigma_{eq} = f(\varepsilon_{eq})$ is the same as the stress-strain relationship under uniaxial tensile loading $\sigma = f(\varepsilon)$. The stress intensity is derived from the von Mises yield criterion, and the strain intensity is defined as [16]:

$$\varepsilon_{eq} = \frac{2}{\sqrt{3}}\sqrt{\left(\varepsilon_z - \varepsilon_\varphi\right)^2 + \left(\varepsilon_\varphi - \varepsilon_x\right)^2 + \left(\varepsilon_x - \varepsilon_z\right)^2} \tag{11}$$

where ε_z, ε_φ and ε_x are the principal strains at a certain point of the cross-section.

The so-called *surface-to-surface* contact elements are recommended to be used in the case of contact of deformable bodies, which are assembled with certain interference. Such elements can be of higher order approximation with inside nodes introduced. This provides

better results for many engineering applications and enables modelling complex, curved shapes of bodies that are in contact. The above contact elements are defined on the surface geometry and need several constants and options to set prior to the analysis. The augmented Lagrangian method was used with contact detection points localised in nodal points in the considered problem. Also, the contact stiffness updated at each iteration step, based on the current mean stress, was applied. The Coulomb friction law was used in the analysis.

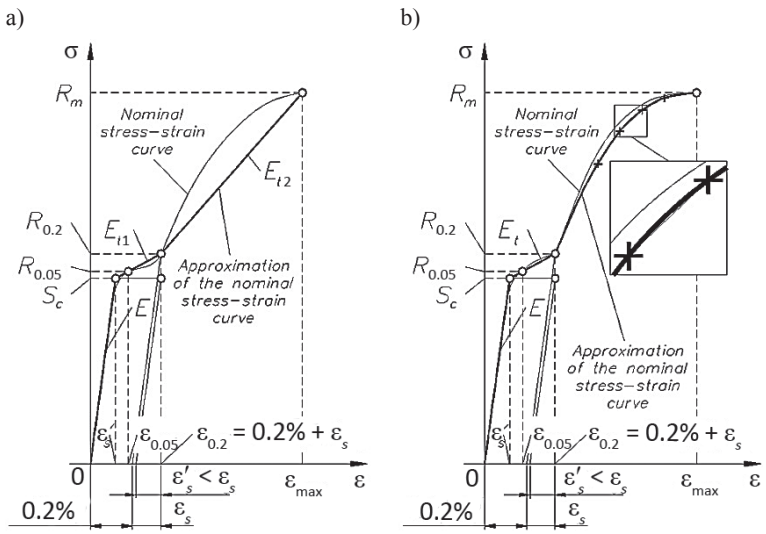

Fig. 7. Approximations of the real stress-strain curves $\sigma = f(\varepsilon)$ (displayed in stretched scale)

In general, the analyzed structure should be modelled as a 3D object, which results in a very big numerical model and demands a lot of time to get the solution. The size of the task can be reduced when the ideal geometry of the junction is presumed. Then, the structure is assumed to be axially symmetric and only a half-part of the cross-section is considered. The high accuracy of numerical results is provided by the application of 8-node quadrilateral axisymmetrical finite elements, which are well-suited for irregular meshes and tasks with elastic and plastic deformations. The finite elements are accompanied with the contact elements introduced on the lines where the contact is expected. Like in the majority of nonlinear problems, the number of applied finite elements should be rather high and the dense meshes should be used in order to keep the solution error within the acceptable range, in particular in the vicinity of the contact zones. The mesh in this area should be dense enough to give satisfying results, while the mesh on the outer unloaded surfaces can be rather rough [15].

In the first numerical approach (FEM 1), the interferences between the gasket and both sectional seats were arranged by means of the thermal method. For the calculation purpose, the gasket was first cooled down and after inserting into the seats and expanding the appropriate interference fits were obtained in the closure. The thermal simulation of the assembly process leads to the same (symmetric) results in displacements, stresses and contact pressure in both half-parts of the axial cross-section.

The second numerical approach (FEM 2) follows the assembly process performed on the stand during the experiment. The nonlinear contact analysis was divided into two steps. In the first step, the gasket was pressed into the bottom sectional seat (supported vertically), while in the second one the upper seat was pressed down until the edges of both seats were in contact. In the second step, the bottom edge of the bottom seat and the bottom edge of the gasket were blocked against the vertical displacement. The symmetry of results, with respect to the middle surface, disappears in this case.

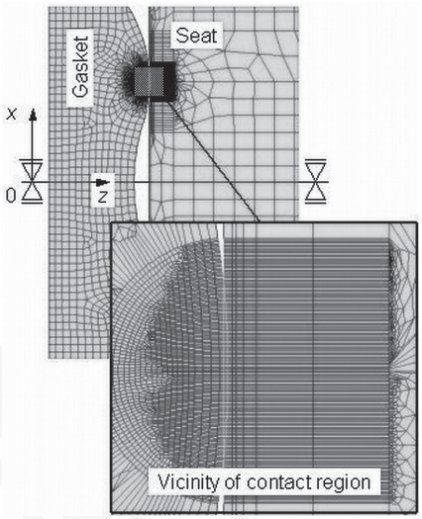

Fig. 8. Example of the mesh of finite elements, division of the closure into parts and illustration of the boundary conditions

Even with the introduced simplifying assumptions and restrictions concerning the geometry and loading, the numerical solution is time consuming and difficult to obtain due to the numerical instability. The size of the finite elements in the anticipated contact zone and the size of the load step should be chosen with particular care in order to avoid convergence problems. Several numerical trials have been carried out to get the final mesh, which is shown in Fig. 8. As a final criterion for the choice of the element size, a compromise between the calculation time and approximation error has been established. The criterion used for the approximation error Δ is based on the comparison between the maximum absolute value of the radial stress $\sigma_{z\,\max}$ and the maximum contact pressure $q_{\max}$ and accepts the mesh for which the discrepancy is less than 5% for each load step [6]:

$$\Delta = \frac{\left|\left|\sigma_{z\max}\right| - q_{\max}\right|}{q_{\max}} 100\% \leq 5\% \tag{12}$$

Distribution of equivalent stress σ_{eq} for the initial interference δ = = 1.0‰ under the load p = 100 MPa at the contact surfaces of the gasket and the seat is shown in Fig. 9.

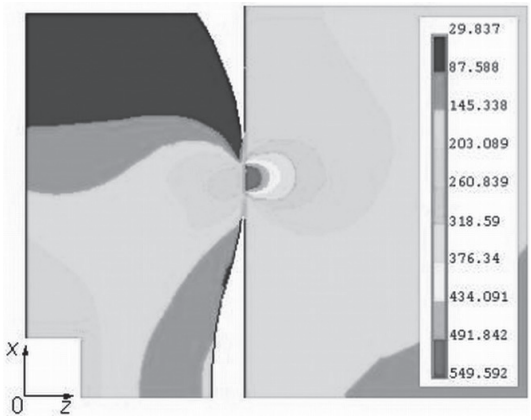

Fig. 9. Distribution of equivalent stress σ_{eq} for the initial interference δ = 1.0‰ under load p = 100 MPa at the gasket-seat contact surfaces

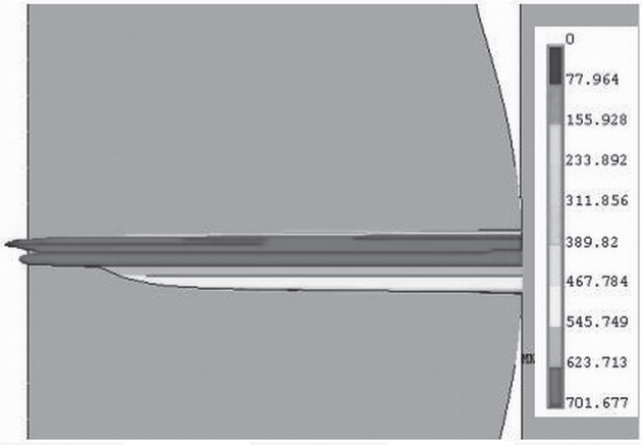

Fig. 10. Example of distribution of contact pressure q in the closure for the initial interference $\delta = 1.0‰$ under load $p = 100$ MPa

An example of the distribution of contact pressure q in the closure is presented in Fig. 10 for the same interference δ and the same operating pressure p. The numerical results are obtained applying FEM 2 procedure for the upper part of the wave-ring gasket, which is assembled in the second step. The friction in contact zones was included in the proposed finite element model with the coefficient of friction assumed $\mu = 0.25$ [3].

5. Definition of gasket dimensionless parameters

The dimensionless variables were applied to investigate the strength and operating properties of wave-ring gaskets. The calculations were based on the simplified analytical shell model of the gasket. The critical section of the gasket is placed at its centre of symmetry, where the equivalent stress σ_{eq} is maximal at the inner radius under the operating pressure (point A in Fig. 3). The strength of the gasket was estimated using the dimensionless parameter σ defined as:

$$\sigma = \sigma_{eq}/R_{0.2\,g} \text{ – dimensionless strength parameter}$$

where $R_{0.2\,g}$ MPa stands for the yield point of the gasket material. The leak tightness of the closure depends on stress q acting at the toroidal wave working surface of the gasket (Fig. 2). The recommendations verified in practice used in the design projects of high-pressure chemical equipment were applied to investigate the leak tightness of the joint. It was assumed that the closure is leak-proof if the average contact pressure $q_{m\,opr}$ satisfies condition (1). The dimensionless parameter ψ:

$$\psi = q_{m\,opr}/2p \text{ – dimensionless leak tightness parameter}$$

was introduced to estimate the functional quality of the closure with respect to non-leakage condition. Dimensionless operating pressure was defined as:

$$\tau = p/R_{0.2\,g} \text{ – dimensionless operating pressure}$$

Another dimensionless variables subjected to change during the analysis were introduced as:

$$\chi = t/h \text{ – dimensionless geometry ratio of the gasket}$$

$$\delta \text{ – relative radial interference (in per milles)}$$

$$\gamma = t/r \text{ – dimensionless average thickness of the gasket}$$

$$\rho = R_1/t \text{ – dimensionless radius of the working wave surface}$$

where all quantities are defined in Figs. 3 and 4. The geometry of the real gasket is presented in Fig. 3 and the dimensions of the analytical model of the gasket used in the analytical approach are shown in Fig. 4.

6. Analysis of gasket strength and operating properties

Detailed analytical calculations were carried out for the dimensions of the gasket, which were applied in the earlier investigations [10], i.e. t = 8.73 mm, r = 56.87 mm, R_1 = 14 mm, $2h$ = 20 mm, $2l$ = 35 mm and $R_{0.2\,g}$ = 260.30 MPa like for the normalised 25CrMo4 material. The average thickness t of the gasket was calculated as the arithmetic mean of its three extreme values, and the average radius r was a result of the assumed thickness t and of the inner radius $ØA$ of the seat (Fig. 3). The thickness coefficient of the seats was set at the maximum admissible value $\beta = 2.00$.

The strength of the gasket and its leak tightness were investigated versus dimensionless operating pressure τ in the range [0, 1], i.e. the maximum operating pressure was assumed to be equal to the yield limit of the gasket material. The analysis was based on the variation of one of the earlier defined geometric or assembly dimensionless parameters of the gasket χ, δ, γ and ρ in the technical acceptable range, while the remaining parameters were kept at a constant mean level. Dimensionless geometry ratio of the gasket was changed in the range χ = 0.06–1.60, relative radial interference was changed in the range δ = 0.5–3.0‰, dimensionless average thickness of the gasket was modified in the range γ = 0.05–0.30 and dimensionless radius of the working wave surface was subjected to variation in the range ρ = 0.5–3.0. The mean values of dimensionless parameters refer to the geometry of the closure used in the experimental investigations χ = 0.8730, δ = 1.0‰, γ = 0.1535 and ρ = 1.6037.

Initial analytical calculations based on the standard thin-walled shell theory [2, 11], and preliminary FEM simulation, lead to the conclusion that the maximum stress appears at the cross-section placed at the gasket's centre of symmetry. The maximum equivalent stress

σ_{eq} appears at this cross-section, which can be seen in Fig. 11. The dimensionless strength parameter σ is presented at four characteristic points versus the dimensionless operating pressure τ: at the inner (σ_i) and at the outer (σ_o) radii of the gasket, in the central cross-section ($x = 0$) and in the extreme cross-section ($x = h$).

Special attention must be paid to the strength of the gasket in assembly conditions and for relatively low pressure τ which occurs during starting of high-pressure equipment. In assembly conditions, the gasket is loaded by shear forces Q_x which are only acting at the supports (Fig. 4). The shear forces are usually of high value as they are caused by the initial radial assembly interference δ. The interference δ must also be of high value because it should ensure the initial leak tightness of the closure necessary while the installation is being filled with the working medium. During the assembly, local plasticity processes occur at the wave surfaces of the gasket. It should be noted that, when the contribution of shear forces Q_x in the loading of the gasket is large and the contribution of the operating pressure τ is small, the maximum strength parameter σ appears at the central cross-section at the outer radius – $\sigma_o(0)$. The above effect can be seen in Fig. 11, where the maximum strength is moving to the inner radius $\sigma_i(0)$ only for the pressure $\tau > 0.08$.

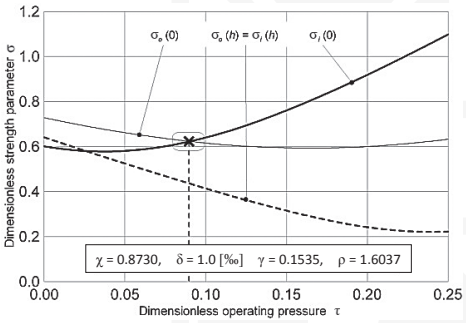

Fig. 11. Dimensionless strength σ at four characteristic points of the gasket versus dimensionless operating pressure τ. Dimensionless parameters χ, δ, γ and ρ fixed at average values

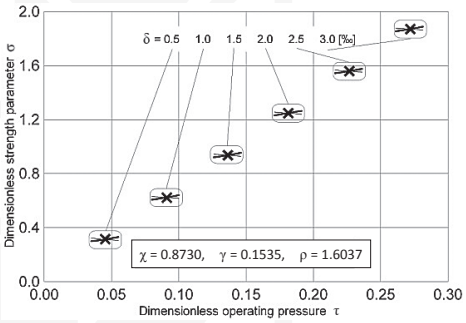

Fig. 12. Dimensionless strength σ of the gasket at the outermost radii versus dimensionless operating pressure τ for different dimensionless parameters δ. Dimensionless parameters χ, γ and ρ fixed at average values

The magnitude of pressure τ, for which the maximum strength parameter σ changes its localisation, depends strongly on the applied initial assembly interference fit δ. The relationship between the strength parameter at the inner radius $\sigma_i(0)$ (bold lines) and the strength parameter at the outer radius $\sigma_o(0)$ (fine lines) and the pressure τ is fragmentarily presented in Fig. 12 for several interference fits. It appears, however, that even for the maximum practical value of the interference fit of the order of 2.5‰ the maximum strength parameter σ shifts from the outer to the inner radius for pressure $\tau > 0.23$. For this reason, the equivalent stress acting at the inner radius was used to estimate the gasket strength.

Dimensionless strength σ at this point for different values of the dimensionless average thickness γ of the gasket and fixed values of χ, δ, and ρ versus pressure τ is shown in Fig. 13.

Permissible range of parameters is for $\sigma \leq 1$ because the loading of the gasket must be lower as the yield limit $R_{0.2\,g}$ of its material. It appears that the influence of the investigated parameter γ on the gasket strength σ is small in the adopted range of other parameters. The closure may be loaded with the pressure $\tau < 0.25$ for which the condition $\sigma \leq 1$ is satisfied.

The influence of the initial assembly interference fit δ on the strength of the gasket is illustrated in Fig. 14. An increase of the interference fit δ produces a simultaneous decrease of the operating pressure τ for which $\sigma \leq 1$. The negative interference fit has an unloading partial effect on the stress distribution caused by pressure τ. The large magnitude of the interference fit δ together with the large value of the thickness coefficient β of the seats cause that for $\delta = 2.0‰$ the strength of the gasket exceeds $\sigma = 1$ in certain places already during the mounting process of the closure.

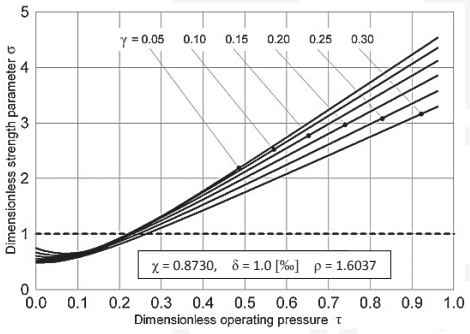

Fig. 13. Dimensionless maximum strength σ of the gasket versus dimensionless operating pressure τ for different dimensionless parameters γ. Dimensionless parameters χ, δ and ρ fixed at average values

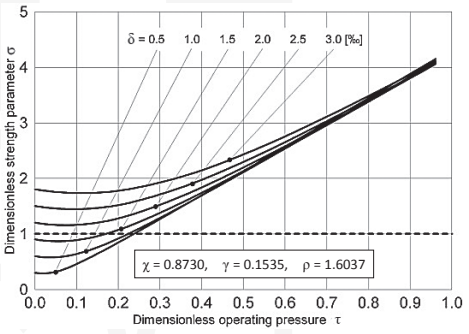

Fig. 14. Dimensionless maximum strength σ of the gasket versus dimensionless operating pressure τ for different dimensionless parameters δ. Dimensionless parameters χ, γ and ρ fixed at average values

The ratio of cross-sectional dimensions χ has a distinct influence on the strength of the gasket. The examination of the relationships in Fig. 15 leads to the conclusion that an increase of the parameter χ from 0.6 to 1.6 results in a significant increase of the gasket load capacity τ.

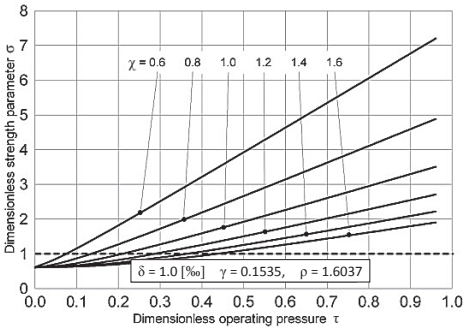

Fig. 15. Dimensionless maximum strength σ of the gasket versus dimensionless operating pressure τ for different dimensionless parameters χ. Dimensionless parameters δ, γ and ρ fixed at average values

It is assumed that because of the highly approximate assumption of the stress distribution in the contact region, leak tightness is preserved for the parameter $\psi \geq 2$. The average stress q_m calculated on the basis of purely elastic Hertz approach is in this case four times greater than the applied operating pressure p. The influence of the dimensionless parameters χ, δ, γ and ρ on leak tightness parameter ψ is presented in Figs. 16–19. The general tendency of leak tightness is to decrease, with an increase of the operating pressure.

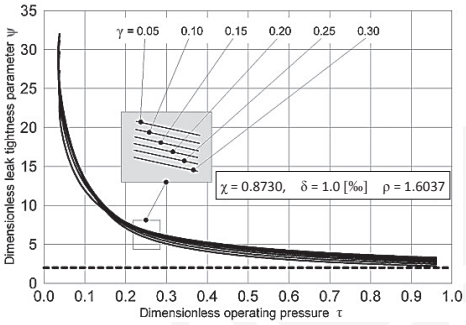

Fig. 16. Dimensionless leak tightness parameter ψ versus dimensionless operating pressure τ for different dimensionless parameters γ. Dimensionless parameters χ, δ and ρ fixed at average values

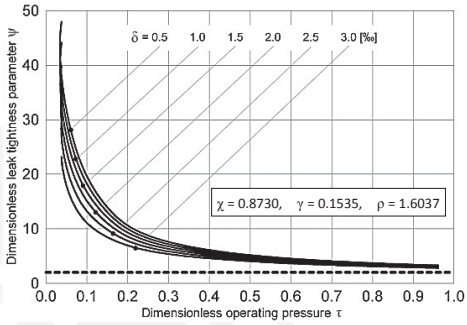

Fig. 17. Dimensionless leak tightness parameter ψ versus dimensionless operating pressure τ for different dimensionless parameters δ. Dimensionless parameters χ, γ and ρ fixed at average values

An increase of parameter γ (an increase of the gasket thickness) has a negative effect (Fig. 16). The examination of the relationships in Figs. 17 and 18 indicates that the variation of parameters δ and χ change distinctly the leak tightness parameter ψ of the joint.

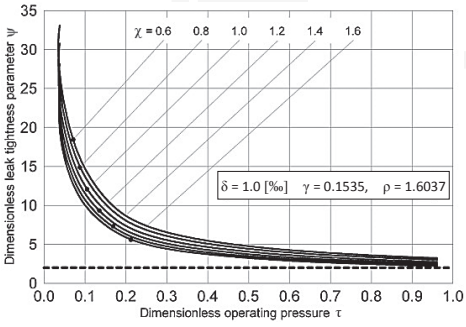

Fig. 18. Dimensionless leak tightness parameter ψ versus dimensionless operating pressure τ for different dimensionless parameters χ. Dimensionless parameters δ, γ and ρ fixed at average values

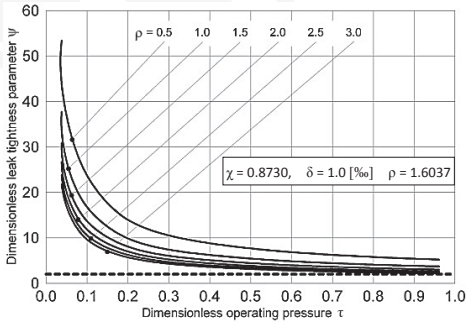

Fig. 19. Dimensionless leak tightness parameter ψ versus dimensionless operating pressure τ for different dimensionless parameters ρ. Dimensionless parameters χ, δ and γ fixed at average values

The variation of parameter ρ connected with the wavy working surface of the gasket produces significant changes in leak tightness (Fig. 19). Too high value of this parameter ($\rho > 3.0$) may be the cause of a loss of leak tightness, in particular for greater values of the operating pressure τ.

All distributions of the dimensionless leak tightness parameter ψ versus dimensionless operating pressure τ presented in Figs. 16–19 are placed considerably beyond the admissible value $\psi = 2$ in the adopted range of the closure parameters. It appears that the non-leakage condition (1) of the joint is satisfied and leak tightness is preserved, in particular for low values of the operating pressure τ.

7. Comparison of the analytical approach with FEM simulation and test results

The experimental results were obtained in the installation state with no operating pressure applied to the joint. The dimensions of the investigated closure are presented in Fig. 3. The gaskets were pressed into their seats and the circumferential and axial strains were measured at the inner surfaces of the gaskets. This is why the comparison of the analytical approach with FEM modelling and test results may be carried out in the assembly conditions only.

Examination of the dimensionless strength parameter σ distributed along the gasket width (Fig. 20) confirms that a change of loading of the gaskets and application of the numerical model FEM 2, similar to real test conditions, makes the numerical results closer to the test results, in particular for small nominal radial interference $\delta = 0.5‰$.

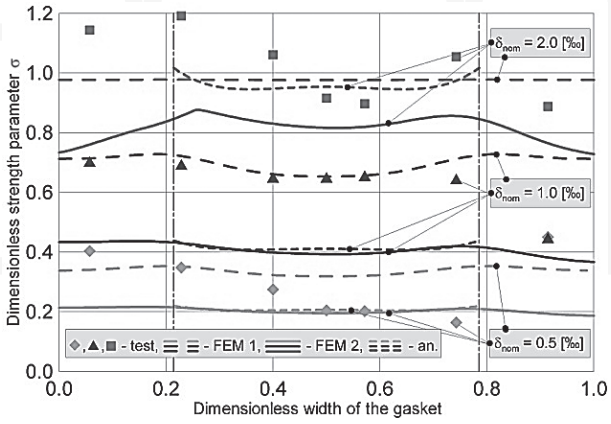

Fig. 20. Dimensionless strength parameter σ at the inner surface of the gaskets versus dimensionless width in assembly conditions ($\tau = 0$). Labels: ♦, ▲, ■ – test results for nominal interferences $\delta = 0.5‰$, 1.0‰ and 2.0‰, respectively. Wide dashed lines – FEM 1 results for nominal interferences, solid lines – FEM 2 results for nominal interferences, narrow dashed lines – analytical results for nominal interferences

Most of the test results are placed in the vicinity of the range received by FEM 2 method and the analytical approach. The greater interferences δ (1.0‰ and 2.0‰) result in respectively

greater differences between FEM 1 and FEM 2 methods and analytical solutions, whereas the test results are located between FEM 1 and analytical results. Investigation of experimental and theoretical strength distributions shown in Fig. 20 leads to the conclusion that FEM 1 method is overestimated and analytical calculations are underestimated with respect to the experiment. The difference increases with the increase of the initial interference.

The dimensionless maximum strength parameter σ at point *A* (Fig. 3) versus dimensionless operating pressure τ is compared in Fig. 21 for the analytical approach and FEM 2 simulation. The numerical calculations were carried out for the thickness coefficient of the seats $\beta = 2.00$. For loading $\tau < 0.3$, the nature of both relationships is similar, although analytical results are considerably greater. Above the yield limit ($\sigma > 1$), the difference rapidly increases, with an increase of the loading. The width of the contact region *e* versus the dimensionless operating pressure τ for the above solutions is presented in Fig. 22. In this case, the relative difference is even greater.

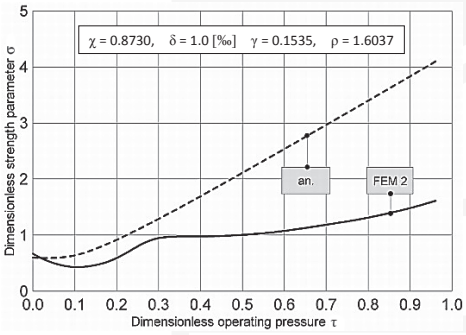

Fig. 21. Dimensionless maximum strength σ of the gasket versus dimensionless operating pressure τ. Comparison of the analytical approach with FEM simulation

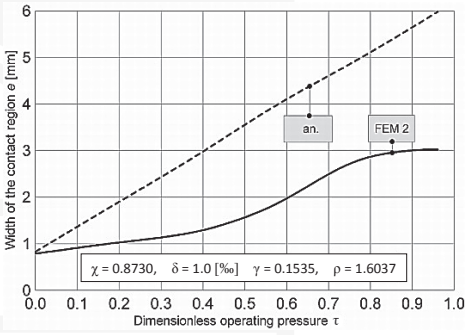

Fig. 22. Width of the contact region versus dimensionless operating pressure τ. Comparison of the analytical approach with FEM simulation

The leak tightness of the joint depends, in particular, on the applied initial assembly interference δ. Visual inspection of the gaskets (Fig. 23) after disassembly indicates that the designed interference must be less than 2.0‰ for the unchanged other parameters of the investigated closure. Too close radial interference fit with respect to the yield limit $R_{0.2\,g}$ of the gasket material was probably the main cause of the serious damage of the working surface. In this case, during the assembly (and disassembly), operation under load in the absence of adequate lubricant the applied interference fit together with a large value of the friction coefficient lead to adhesive wear [4]. The original adhesion theory postulated that all asperity contacts would result in yielding and adhesion due to the high stresses present.

When clean surfaces are pressed against one another under load, some of the asperities in contact will tend to adhere to one another due to the attractive forces between the surface atoms of the two materials. As sliding between the surfaces is introduced, these adhesions are broken, either along the original interface, or along a new plane through the material of the asperity peak. In the latter case, a piece of one part is transferred to another part, causing

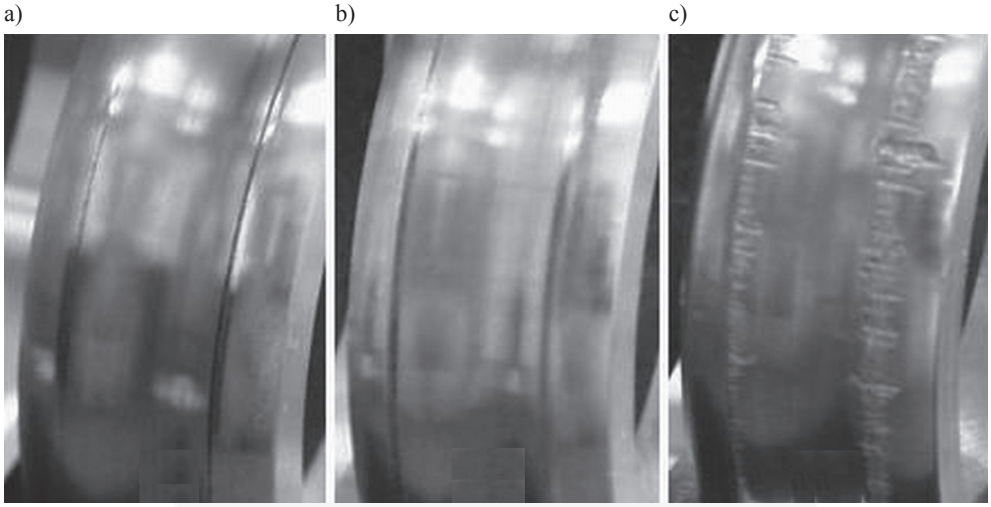

Fig. 23. The gaskets after disassembly. Interferences δ: a) 0.5‰; b) 1.0‰; c) 2.0‰. Note the contact traces

surface disruption and damage. Sometimes, a particle of one material will be broken free and become debris in the interface, which can then scratch the surface and plough furrows in both parts. This damage is called scoring or scuffing of the surface.

8. Final remarks

The simplified analytical approach, based on the shell theory, was applied to investigate the influence of certain geometric, material and assembly parameters on the strength and leak properties of high-pressure closure with a wave-ring gasket. The analytical solution was verified by FEM modelling and by an experiment. On the basis of the obtained results, certain general conclusions and recommendations may be formulated with respect to the safety of the joint.

Because of specific working features of the wave-ring gasket, the yield point of its material must be relatively lower than that of the seat. Reactor vessel walls and its heads, as well as the pipelines designed for high-pressure applications, are manufactured out of high-carbon chromium-nickel-molybdenum steel. The yield stress of such material usually exceeds $R_{0.2\,g} > 750$ MPa and possible Rockwell hardness number is of the order of 45–48. The corresponding wave-ring gasket should be made of a material of which Brinell hardness number is less than 250–280 BHN and the yield stress is approximately $R_{0.2\,g} = 400$ MPa. Acceptable operating pressure should be of the order of $p = 250$–300 MPa. Application of a higher operating pressure must be preceded with a detailed stress-strain analysis of the gasket and earlier considerations with respect to leak tightness.

The strength of a wave-ring gasket cannot be improved significantly through the change of the dimensionless parameter γ, however, greater loading capacity may be obtained through

an increase of parameter χ. The increase of parameter χ to 1.6 produces an increase of the parameter τ to 0.43.

Special attention should be paid to the magnitude of the initial assembly interference fit δ. The interference fit less than 0.5‰ may cause leakage of installation at the start, in particular for the joints of large diameters for which it is hard to provide precise dimensional accuracy. On the other hand, the interference fit exceeding 2.5‰ appears too large because it insignificantly improves leak tightness, but it produces significant damage of the working surface during the assembly of the joint. The interference fit δ = 1.0–2.0‰ is recommended to the closures with wave-ring gaskets for the adopted data.

The analytical computational model of the closure may be convenient to proceed an initial analysis. A large number of simple calculations can be carried out for different geometry of the gasket, different material properties and assembly requirements. It should be noted that a comparison of experimental and theoretical results reveals that the analytical calculations are underestimated with respect to the tests. The final parameters of the closure may then be determined in the detailed FEM verification, which is closer to the experimental results.

The experimental investigations indicate that gasket installation and replacement operations should be carried out with extreme precision. Attention must be paid to the exact alignment of the gasket with respect to the seat, and above all, in closures with a large diameter. As a conclusion of the experimental investigations, it should be noted that the assembly process realised by means of the expanding technique (thermal method) is advantageous with respect to the mounting process in which the gasket is pressed into the seat. Inaccurate sliding process may result in scoring of the wave surface of the gasket.

Moreover, the manufacturing process of wave-ring gaskets must ensure high dimensional accuracy, in particular with respect to the wave working surface, as the effective interference fit depends on this accuracy. The average nominal diameters of approximately 200 mm require the IT6–IT7 grade of tolerance and the roughness number of R_a = 0.16 μm seems to be sufficient.

References

[1] Freeman A.R., *Gaskets for high-pressure vessels*, [in:] *Pressure Vessel and Piping Design. Collected Papers 1927–1959*, 1960, 165-168.

[2] Kozłowski T., *Theory of plasticity*, Arkady, Warsaw 1968.

[3] Krukowski A., Tutaj J., *Deformable joints*, PWN, Warsaw 1987.

[4] Norton R.L., *Machine design. An integrated approach*, Pearson Education LTD, New Jersey 2006.

[5] Ryś J., Szybiński B., Trojnacki A., *Computational model of metal high-pressure wave-ring gasket*, Technical Transactions, series Mechanics, Vol. 11, 2006, 63-87.

[6] Stein E., *Error-controlled adaptive finite elements in solid mechanics*, John Wiley&Sons, LTD, West Sussex 2003.

[7] Szybiński B., Trojnacki A., *Experimental verification of stress-strain analysis of metal wave-ring gasket*, Mechanical Review, Vol. 7-8'11, 2011, 50-57.

[8] Szybiński B., Trojnacki A., *Experimental investigations of metal high-pressure wave-ring gasket*, [in:] J.F.S. Gomes, S.A. Meguid (Eds): *Recent Advances in Integrity-*

Reliability-Failure, Proc. of the 4th Int. Conf. on Integrity, Reliability and Failure, Funchal 2013, 805-806.

[9] Szybiński B., Trojnacki A., *Experimental investigations of metal high-pressure wave-ring gasket*, [in:] J.F.S. Gomes, S.A. Meguid (Eds): Proc. IRF2013, 4th Int. Conf. Integrity-Reliability-Failure, Funchal 2013, 1-17.

[10] Szybiński B., Trojnacki A., *Analytical and numerical solutions of metal high-pressure wave-ring gasket and comparison with experimental results*, The Archive of Mechanical Engineering, Vol. LXII(1), 2015, 19-44.

[11] Timoshenko S., Woinowsky-Krieger S., *Theory of plates and shells*, Arkady, Warsaw 1962.

[12] Trojnacki A., *Druckstandfestigkeit und Betriebseigenschaften von Doppelwellendichtungen*, Chemie Ingenieur Technik, Vol. 83(3), 2011, 377-385.

[13] Walczak J., *Strength of materials and elements of elasticity and plasticity*, PWN, Warsaw 1973.

[14] Woźniak C. (Ed), *Technical Mechanics*, Vol. VIII, *Mechanics of elastic plates and shells*, PWN, Warsaw 2001.

[15] Wriggers P., *Computational contact mechanics*, John Wiley&Sons, Ltd., West Sussex 2002.

[16] Życzkowski M. (Ed), *Technical Mechanics*, Vol. IX, *Strength of structural elements*, PWN, Warsaw 1988.

[17] ANSYS, *Release 8.0*, Analysis System Inc., Swanson 2003.

[18] Realization of technical documentation of the reactor 41/42 V-7 for the polyethylene installation. Report TPP–5 Cracow University of Technology, Cracow 2000.